Stable water isotopes and accumulation rates in the Union Glacier region, West Antarctica over the last 35 years

Kirstin Hoffmann[1, 2], Francisco Fernandoy[3], Hanno Meyer[2], Elizabeth R. Thomas[4], Marcelo Aliaga[3],
Dieter Tetzner[5], Johannes Freitag[6], Thomas Opel[7,2], Jorge Arigony–Neto[8], Christian Florian Göbel[8],
5 Ricardo Jaña[9], Delia Rodríguez Oroz[10], Rebecca Tuckwell[4], Emily Ludlow[4], Joseph R. McConnell[11],
Christoph Schneider[1]

[1]Department of Geography, Humboldt University Berlin, Unter den Linden 6, Berlin, 10099, Germany
[2]Alfred Wegener Institute, Helmholtz Centre for Polar and Marine Research, Research Unit Potsdam, Telegrafenberg A43,
Potsdam, 14473, Germany
10 [3]Facultad de Ingeniería, Universidad Nacional Andrés Bello, Viña del Mar, 2531015, Chile
[4]Ice Dynamics and Paleoclimate, British Antarctic Survey, High Cross, Cambridge, CB3 0ET, United Kingdom
[5]Department of Earth Sciences, University of Cambridge, Downing Street, Cambridge, CB2 3EQ, United Kingdom
[6]Alfred Wegener Institute, Helmholtz Centre for Polar and Marine Research, Am Alten Hafen 26, Bremerhaven, 27568,
Germany
15 [7]Department of Geography, Permafrost Laboratory, University of Sussex, Falmer, Brighton, BN1 9QJ, United Kingdom
[8]Instituto de Oceanografia, Universidade Federal do Rio Grande, Av. Itália, km 8, CEP 96201900, Rio Grande, RS, Brazil
[9]Departamento Científico, Instituto Antártico Chileno, Plaza Muñoz Gamero 1055, Punta Arenas, Chile
[10]Facultad de Ingeniería, Universidad del Desarrollo, Avenida Plaza 680, Santiago, Chile
[11]Division of Hydrologic Sciences, Desert Research Institute, 2215 Raggio Parkway, Reno, NV 89512, USA

Correspondence to: Kirstin Hoffmann (Kirstin.Hoffmann@awi.de)

Abstract

West Antarctica is well-known as a region that is highly susceptible to atmospheric and oceanic warming. However, due to
the lack of long–term and in–situ meteorological observations little is known about the magnitude of the warming and the
25 meteorological conditions in the region at the intersection between the Antarctic Peninsula (AP), the West Antarctic Ice Sheet
(WAIS) and the East Antarctic Ice Sheet (EAIS). Here we present new stable water isotope data (δ^{18}O, δD, d excess) and
accumulation rates from firn cores in the Union Glacier (UG) region, located in the Ellsworth Mountains at the northern edge
of the WAIS. The firn core stable oxygen isotope composition reveals no statistically significant trend for the period 1980-
2014 suggesting that regional changes in near-surface air temperature have been small during the last 35 years. As for stable
30 oxygen isotopes no statistically significant trend has been found for the d excess suggesting overall little change in the main
moisture sources and the origin of precipitating air masses for the UG region at least since 1980. Backward trajectory modelling
revealed the Weddell Sea sector to be the likely main moisture source region for the study site throughout the year. We found
that mean annual δ–values in the UG region are correlated with sea ice concentrations in the northern Weddell Sea, but are not
strongly influenced by large-scale modes of climate variability such as the Southern Annular Mode (SAM) and the El Niño–
35 Southern Oscillation (ENSO). Only mean annual d excess values are weakly positively correlated with the SAM.

On average snow accumulation in the UG region amounts to about 0.25 m w. eq. a^{-1} between 1980 and 2014. Mean annual snow accumulation has slightly decreased since 1980 (–0.001 m w.eq.a^{-1}, p–value = 0.006). However, snow accumulation at UG is neither correlated with sea ice nor with SAM and ENSO confirming that the large increases in snow accumulation observed on the AP and in other coastal regions of Antarctica have not extended inland to the Ellsworth Mountains. We

5 conclude that the UG region – located in the transition zone between the AP, the WAIS and the EAIS – is exhibiting rather East than West Antarctic climate characteristics.

1. Introduction

The Antarctic Peninsula (AP) and the West Antarctic Ice Sheet (WAIS) have gained scientific interest as both regions have

10 been experiencing significant atmospheric and oceanic changes during recent decades. The WAIS is considered as one of the fastest warming regions on Earth based on the analysis of meteorological records (Steig et al., 2009; Bromwich et al., 2013) and ice cores (Steig et al., 2013). Time series of near–surface air temperature from weather stations (Turner et al., 2005; Vaughan et al., 2003) as well as stable water isotope records from ice cores (Thomas et al., 2009; Abram et al. 2011) provide evidence that the AP has warmed by more than 3°C since the 1950s.

15 The mechanisms and factors forcing the anomalously strong and rapid warming of the AP and the WAIS have been widely discussed: For the AP the warming process has been linked to the shift of the Southern Annular Mode (SAM) towards its positive phase during the second half of the 20th century (e.g. Thompson and Solomon, 2002; Gillett et al., 2006; Marshall, 2006; Marshall et al., 2007;). The SAM is the principal zonally–symmetric mode of atmospheric variability in extra–tropical regions of the Southern Hemisphere (Limpasuvan and Hartmann, 1999; Thompson and Wallace, 2000; Turner, 2004). The

20 positive phase of the SAM is characterized by decreased geopotential height over the polar cap, but increased geopotential height over the mid–latitudes. This leads to a strengthening and poleward shift of the mid–latitude westerlies over the Southern Ocean and hence to increased cyclonic activity and warm air advection towards Antarctic coastal regions (Thompson and Wallace, 2000; Thompson and Solomon, 2002; Turner, 2004; Gillett et al., 2006). Consequently, a positive (negative) SAM is associated with a warming (cooling) on the AP and anomalously low (high) temperatures over eastern Antarctica and the

25 Antarctic plateau (Thompson and Wallace, 2000; Thompson and Solomon, 2002; Gillett et al., 2006). The recent shift of the SAM towards its positive phase has been attributed to the increase of anthropogenic greenhouse gas concentrations in the atmosphere and to stratospheric ozone depletion (Thompson et al., 2011; Gillett et al., 2008), but also to locally confined sea–ice loss (Turner et al., 2013).

The exceptional rapid warming of the WAIS has been suggested to be driven by sea surface temperature (SST) anomalies in

30 the central and western (sub)tropical Pacific (e.g. Schneider et al., 2012; Ding et al., 2011; Steig et al., 2013; Bromwich et al., 2013). It further seems to be linked to the recent deepening of the Amundsen Sea Low (ASL) influencing meridional air mass and heat transport towards West Antarctica (Bromwich et al., 2013; Hosking et al., 2013; Raphael et al., 2015). Changes in the absolute depth of the ASL are strongly related to the phase of the El Niño–Southern Oscillation (ENSO) and the SAM (Raphael et al., 2015). ENSO is the largest climatic cycle on Earth on decadal and sub–decadal time scales originating in the tropical

Pacific. ENSO directly influences the weather and oceanic conditions across tropical, mid– and high–latitude areas on both hemispheres (Karoly, 1989; Diaz and Markgraf, 1992; Diaz and Markgraf, 2000; Turner, 2004; L'Heureux and Thompson, 2006).

However, current trends in Antarctic climate and their drivers are still not completely understood, especially on regional scales.

5 Turner et al. (2016) revealed that temperatures on the AP have decreased since the late 1990s, due to increased cyclonic activity in the northern Weddell Sea. Thomas et al. (2013) showed that the warming in West Antarctica at the end of the 20th century was not unprecedented in the past 300 years. In addition, the East Antarctic Ice Sheet (EAIS) has rather experienced a slight cooling during recent decades, in line with the occurrence of a more positive SAM (Turner et al., 2005; Stenni et al., 2017). Therefore, data on meteorological parameters such as air temperature, precipitation (accumulation rates), moisture sources and

10 transport pathways of precipitating air masses are vital to assess past and recent changes of Antarctic climate. Direct observations of these parameters are lacking, particularly in the interior of the Antarctic continent, and, thus proxy data derived from firn and ice cores, e.g. stable water isotopes, provide important information on past and recent climate variability on local to regional scales (Thomas and Bracegirdle, 2015). For the region at the intersection between the AP, the WAIS and the East Antarctic Ice Sheet (EAIS) data is generally sparse, and little or no long–term meteorological data are available from this part

15 of the Antarctic continent (Stenni et al., 2017; Thomas et al., 2017). The region is located at the transition to the Ronne– Filchner Ice Shelf, for which a recent modelling study suggests its susceptibility to destabilization and disintegration under a warming climate (Hellmer et al., 2012; Hellmer et al., 2017), as already observed for ice shelfs around the AP and the WAIS (e.g. Pritchard and Vaughan, 2007; Cook and Vaughan, 2010; Scambos et al., 2014; Rignot et al., 2014; Joughin and Alley, 2011).

20 This study aims to improve our understanding of climate change at the intersection between the AP, the WAIS and the EAIS based on firn–core stable water isotope data from the Union Glacier (UG) region, located in the Ellsworth Mountains at the northern edge of the WAIS (Fig. 1a). Union Glacier (79°46' S, 83°24' W; 770 m above sea level [asl.]) is one of the major outlet glaciers within the Ellsworth Mountains and flows into the Ronne–Filchner Ice Shelf in the Weddell Sea sector of Antarctica. It is composed of several glacier tributaries – the main ones being Union and Schanz Glaciers – covering an

25 estimated total area of 2561 km^2. UG has a total length of 86 km, a maximum ice thickness of 1540 m and a maximum depth of the snow–ice boundary layer of 120 m (Rivera et al., 2014) The subglacial topography of the glacier valley is smooth with U–shaped flanks and the bedrock is located below sea level (–858 m; Rivera et al., 2014).

In this study we use high–resolution data on the density and stable water isotope composition of firn cores drilled at various locations in the UG region for reconstructing accumulation rates and inferring recent changes in meteorological parameters

30 such as air temperature on local to regional scales. We further investigate how these variables are related to temporal changes of moisture source regions, sea ice extent and concentration (SIE and SIC) and atmospheric modes such as SAM and ENSO. Backward trajectory analyses are applied to determine potential source regions and transport pathways of precipitating air masses reaching the UG region. We aim to conclude on whether and to what extent the UG region and surrounding areas are

experiencing the same strong and rapid warming as observed for the neighbouring AP in the north and the WAIS in the south, respectively.

2. Data and Methodology

2.1 Fieldwork, sample processing and analysis

Two glaciological field campaigns were conducted in the UG region in austral summers 2014 and 2015. Here we examine six firn cores retrieved, using a portable solar–powered and electrically–operated ice core drill (Backpack Drill; icedrill.ch AG), at different locations ranging between 760 m asl. and 1900 m asl. in altitude: GUPA–1, DOTT–1, SCH–1, SCH–2, BAL–1 and PASO–1 (Fig. 1b). Details on the drill locations and basic core characteristics are given in Table 1.

For cores BAL–1 and PASO–1 high–resolution (< 1 mm) density profiles were obtained using X–ray microfocus computer tomography (ICE–CT; Freitag et al., 2013) at the ice–core processing facilities of AWI Bremerhaven. The cores were sampled at 2.5 cm resolution and analysed for stable water isotopes using a cavity ring–down spectrometer (L2130–i; Picarro Inc.) coupled to an auto–sampler (PAL HTC–xt; CTC Analytics AG) at the Stable Isotope Laboratory of AWI Potsdam. Stable water isotope raw data was corrected for linear drift and memory effects following the procedures suggested by van Geldern & Barth (2012) using six repeated injections per sample from which the first three were discarded. The drift– and memory–corrected isotopic compositions were then calibrated with a linear regression analysis using four different in–house standards that have been calibrated to the international VSMOW2 (Vienna Standard Mean Ocean Water)/SLAP2 (Standard Light Antarctic Precipitation) scales. Stable water isotope ratios are reported in per mil (‰) versus VSMOW2. Precision of the measurements is better than 0.08‰ for $\delta^{18}O$ and 0.5‰ for δD.

For cores GUPA–1, DOTT–1, SCH–1 and SCH–2 density profiles were constructed by section–wise determining the core volume and weight. Accordingly, average resolution of density profiles is 25 cm for GUPA–1, 40 cm for DOTT–1, 27 cm for SCH–1 and 78 cm for SCH–2. Cores GUPA–1, DOTT–1 and SCH–1 were then sampled at 5 cm resolution for stable water isotope analysis carried out at the Stable Isotope Laboratory of UNAB in Viña del Mar, Chile. For the measurements an off–axis integrated cavity output spectrometer (TLWIA 45EP; Los Gatos Research) was used with a precision being better than 0.1‰ for $\delta^{18}O$ and 0.8‰ for δD (Fernandoy et al., 2018). Each sample was measured using ten repeated injections from which the first four were discarded. Stable water isotope raw data was corrected for linear drift and memory effects and then normalized to the VSMOW2/SLAP2 scales using the software LIMS (Laboratory Information Management System; Coplen & Wassenaar, 2015). For data normalization three different in–house standards and one USGS standard (USGS49) calibrated to the international VSMOW2/SLAP2 scale were used.

Core SCH–2 was analysed at the British Antarctic Survey (BAS). Stable water isotopes were determined at 5 cm resolution using a Picarro L2130–i analyser with measurement precision of 0.08‰ for $\delta^{18}O$ and 0.5‰ for δD. Major ions (Cl^-, NO_3^-, SO_4^{2-}, MSA^-, Na^+, K^+, Mg^{2+}, Ca^{2+}) were measured at 5 cm resolution using a Dionex reagent–free ion chromatography system (ICS–2000). Furthermore, longitudinal subsections of the core (32 mm x 32 mm in size) were melted continuously on a chemically inert, ultra–clean melt head to measure electrical conductivity, dust and H_2O_2 at high resolution (~1 mm;

Continuous Flow Analysis [CFA]); McConnell et al., 2002). In addition, core PASO–1 was analysed for liquid conductivity, H_2O_2, NO_3^-, NH_4^+, Black Carbon and various chemical elements at the Trace Chemistry Laboratory of the Desert Research Institute (DRI) according to methods described in Röthlisberger et al. (2000), McConnell et al. (2002) and McConnell et al. (2007). Chemical elements, of which Na and S are used for core chronology, were measured using two Thermo Finnigan Element2 ICP–MS instruments.

Based on the corrected and calibrated $\delta^{18}O$ and δD values, the d excess was calculated (d excess = $\delta D - 8 * \delta^{18}O$; Dansgaard, 1964) and a co–isotopic relationship ($\delta D = m * \delta^{18}O + n$) was derived for each core. Since there is no recent precipitation stable water isotope data available for the UG region, a Local Meteoric Water Line (LMWL) was inferred from the co–isotopic relationships of all cores.

2.3 Dating of firn cores and time series construction

Firn cores SCH–2 and PASO–1 were dated using annual layer counting (ALC) of stable water isotopes and chemical parameters: Methanesulfonic acid (MSA), SO_4^{2-}, the Cl/Na–ratio and H_2O_2 for SCH–2 (Fig. 2) and nssS (non–sea salt S) and the nssS/ssNa (sea–salt Na)–ratio for PASO–1 as these parameters exhibit clear seasonal alternations between highest and lowest values. For the dating of PASO–1 the signal of the Mt. Pinatubo eruption (1991) could be clearly identified, especially in the nssS record and, hence, was used as additional tie point (Fig. 3). Cores GUPA–1, DOTT–1, SCH–1 and BAL–1 were dated based on ALC of stable water isotopes and matching to the SCH–2 age scale. The estimated error associated to ALC is ±1 year for cores dated with glacio–chemistry and ± 2 years for cores dated with stable water isotopes only.

Snow accumulation rates at the firn core sites were determined and converted to meters of water equivalent per year (m w.eq.a^{-1}) based on measured densities (S1).

Composite stable water isotope and accumulation records were constructed for the entire UG region by combining time series of annually averaged stable water isotopes and accumulation rates of the individual firn cores (non–standardized and standardized; Stenni et al., 2017). Linear trends were calculated and tested for their significance using the non–parametric Mann–Kendall and Sen slope (s) estimator trend test (Mann, 1945; Kendall, 1975; Sen, 1968) with correction for autocorrelation according to Yue & Wang (2004).

2.4 Meteorological database and backward trajectory analysis

Meteorological data from an AWS located at the UG ice runway (79°47' S, 82°53' W, 705 m asl.; Fig. 1b) covers a 4–year period from 1st February 2010 to 8th February 2014. The AWS (station: Wx7) records near–surface air temperature, wind speed, wind direction, relative humidity and air pressure every ten minutes. Additionally, hourly–resolved data of the same meteorological parameters are available from a second AWS (station: Arigony) operated on Union Glacier (79°46' S, 82°54' W, 693 m asl.; Fig. 1b) covering the period from 14th December 2013 to 29th March 2018. Since differences between the Wx7 and the Arigony records are small for all meteorological parameters throughout the overlapping period (14th December 2013 to 8th February 2014), the two datasets were combined in order to expand the meteorological record.

In addition, we used fields of near–surface air temperature (2 m), precipitation–evaporation and geopotential heights (850 mbar) from the European Centre for Medium–Range Weather Forecasts (ECMWF) Interim Reanalysis (ERA–Interim; 1979 onwards; Dee et al., 2011; available at: https://www.ecmwf.int/en/forecasts/datasets/archive–datasets/reanalysis–datasets/era–interim) for comparison with UG composite records of stable water isotopes and accumulation. Annually–averaged stable

5 water isotopes and accumulation rates were also related to time series of climate modes such as SAM and ENSO as well as to SIE and SIC in order to identify dominant drivers of potential climate variability in the UG region. We used the Marshall SAM Index (Marshall, 2003) as indicator for the prevailing SAM phase (available at: https://legacy.bas.ac.uk/met/gjma/sam.html) and the Multivariate ENSO Index (MEI; Wolter and Timlin, 1993, 1998) as indicator for the occurrence and strength of El Niño and La Niña events (available at: https://www.esrl.noaa.gov/psd/enso/mei/table.html).

10 Mean monthly SIE for different Antarctic sectors (Weddell Sea: 60°W–20°E; Indian Ocean: 20°E–90°E; Western Pacific: 90°E–160°E; Ross Sea: 160°E–130°W; Bellingshausen–Amundsen Sea: 130°W–60°W) was obtained from the National Aeronautics and Space Administration (NASA; Cavalieri et al., 1999, 2012; available at: https://neptune.gsfc.nasa.gov/csb/index.php). Note that these data are only available for the period 1979-2012. Satellite–derived SIC data was acquired from the National Snow and Ice Data Center (NSIDC). The data set NSIDC–0079 – Bootstrap

15 SIC from Nimbus–7 SMMR and DMSP SSM/I–SSMIS, Version 3 – with a spatial resolution of 25 km x 25 km was used (available at: https://nsidc.org/data/nsidc–0079; Comiso, 2017). Spatial and cross–correlation analyses with UG time series were carried out calculating Pearson correlation coefficients and p–values at the 95% confidence level. ERA–Interim reanalysis data were annually averaged and detrended before the analyses.

We performed backward trajectory analysis using the Hybrid Single Particle Lagrangian Integrated Trajectory (HYSPLIT)

20 model (Draxler and Hess, 1998; Stein et al., 2015; available at: https://ready.arl.noaa.gov/index.php) in order to determine potential moisture source regions and transport pathways of precipitating air masses for the UG region. ERA–Interim time series of daily precipitation extracted for the period 2010–2014 (resolution: 0.75°x0.75°; available at: http://apps.ecmwf.int/datasets/data/interim–full–daily/levtype=sfc/) served as input data for the calculation of 3–day backward trajectories. In total backward trajectories were calculated for 210 single precipitation events occurring in the period 2010–

25 2014, and subdivided into their respective seasons (DJF, MAM, JJA and SON).

3. Results

3.1 Meteorological data

The mean daily air temperature for the composite record of near–surface air temperature (Fig. 4) was –21.3°C with an absolute

30 minimum of –46.8°C recorded on 17 July 2017 and an absolute maximum of +3.3°C measured on 21 February 2013. Daily air temperatures are highest during December and January with mean values of –9.2°C and –9.1°C, respectively, and lowest from April to September with mean values below –25°C. The coldest month of the whole composite record period (2010–2018) is July with a mean air temperature of –28.8°C. Daily wind speeds have a mean value of 6.9 m/s with a predominant

direction from SW (220°). The maximum wind speed recorded was 29.7 m/s. Generally (> 75%), wind speeds are higher than 1.2 m/s. These observations are in line with those made by Rivera et al. (2014) for the period 2008–2012.

3.2 Firn core age model

5 Stable water isotope profiles ($\delta^{18}O$) of the six firn cores are displayed with respect to depth in S2. Data gaps in GUPA–1, DOTT–1 and SCH–1 are due to leaking sample bags (GUPA–1: 2 samples; DOTT–1: 3 samples; SCH–1: 2 samples). The number of years identified in each core by ALC and the respective period covered is summarized in Table 2. Core DOTT–1 (16 years, 1999–2014) exhibits the shortest and PASO–1 (43 years, 1973–2015) he longest record. Note that for age–model construction of GUPA–1 two years (1990, 2001) and of BAL–1 three years (1981, 1983, 1994) were identified by linear

10 interpolation due to smoothing of the stable water isotope records in the respective core sections. Furthermore, for SCH–1 the first year (1986) was identified by linear extrapolation at the lower end of the core. Furthermore, for all cores the last year (either 2014 or 2015) was excluded from the analysis as it is incomplete.

3.3 Firn core stable water isotopes and accumulation rates

15 The mean isotopic composition of the six firn cores ranges from –36.6 ‰ (PASO–1) to –29.9 ‰ (DOTT–1) for $\delta^{18}O$ and from–285.9 ‰ (PASO–1) to –233.1 ‰ (DOTT–1) for δD, respectively (Table 1). Absolute minimum δ–values are found in GUPA–1, absolute maximum δ–values in DOTT–1. Note that the results for GUPA–1 have to be handled with caution as this core was drilled next to the UG field camp and ice–landing strip. Therefore, snow relocation effects due to wind drift and/or human activities (e.g. runway maintenance) might have biased its stable water isotope composition. This is also indicated by

20 less pronounced seasonal alternations in the GUPA–1 isotope record (S2). Despite different drill locations and altitudes, the range in mean d excess values of the six cores is small (from 4.9 ‰ [SCH–2] to 7.0 ‰ [PASO–1]). The slope of the co–isotopic relationship (Table 1 and Fig. 5a-g) is close to that of the Global Meteoric Water Line (GMWL; Craig, 1961) for all cores. Hence, the meteoric origin of the stable water isotope signal is preserved during moisture transport and snow deposition at the study site (Clark and Fritz, 1997). For all cores $\delta^{18}O$ and δD values are highly correlated ($R^2 \geq 0.98$) with the largest

25 variation in d excess observed for SCH–2 (range: –5.6 ‰ and 17.2 ‰). The LMWL of the UG study region was determined as $\delta D = 8.02*\delta^{18}O + 6.57$ ($R^2 = 0.99$; Fig. 5g).

Highest mean accumulation rates (≥ 0.28 m w.eq.a^{-1}) were found for DOTT–1and SCH–2, despite the site of SCH–2 being located further inland and at about 750 m higher altitude compared to DOTT–1 (Table 1 and Fig. 1b). Lowest mean accumulation occurs at the GUPA–1 and PASO–1 sites (~0.18 m w.eq.a^{-1}). In general, annual minimum accumulation ranges

30 between 0.1 and 0.2 m w.eq.a^{-1} and annual maximum accumulation reaches values of ≥ 0.3 m w.eq.a^{-1} with the absolute maximum found at the SCH–2 site in 1985 (0.47 m w.eq.a^{-1}). However, in the same year accumulation reaches an absolute minimum of 0.08 m w.eq.a^{-1} at the PASO–1 site (Fig. 6).

4. Discussion

4.1 Spatial and temporal variability of firn core stable water isotope composition and relation to sea ice and climate modes

4.1.1 Spatial and temporal variability of stable water isotopes

Prominent maxima in $\delta^{18}O$–time series of UG firn cores are found in 1991, 1997, 2002, 2006 and 2007 (Fig. 7). The above–average warm summer in 2002 is the only maximum found in all cores. Prominent minima occur – although not visible in all cores – in the years 1995, 2001, 2004, 2010 and 2014. In the following, core GUPA–1 is excluded from statistical evaluation due to the likely biasing and smoothing of its stable water isotope record as a consequence of its site specifications. From the inter–comparison of mean, minimum and maximum values of $\delta^{18}O$ annual means for the overlapping period (1999–2013; Table 1 and S3), a depletion of the stable water isotope composition with increasing height ("altitudinal effect") and distance from the sea ("continentality effect") has been detected as expected for a Rayleigh distillation process (Clark and Fritz, 1997). Time–series analysis of $\delta^{18}O$ annual means (S3) reveals positive trends for SCH–1 (s = +0.039 ‰ a^{-1}) and BAL–1 (s = +0.054 ‰ a^{-1}), whereas for DOTT–1 (s = –0.071 ‰ a^{-1}), SCH–2 (s = –0.011 ‰ a^{-1}) and PASO–1 (s = –0.009 ‰ a^{-1}) the $\delta^{18}O$ trend is negative. However, only the positive trends for SCH–1 and BAL–1 are statistically significant (α = 0.05, p–value < α; p–value (SCH–1) = 0.028; p–value (BAL–1) < 0.0001).

The individual firn cores are well correlated with each other (S4). Hence, an overall mean $\delta^{18}O$–record (UG $\delta^{18}O$–stack) has been constructed, both for non–standardized and standardized annually averaged data, spanning the period that comprises at least three core records per year (1980–2014; excluding GUPA-1; Fig. 8). This allows to draw a more regional picture of the isotopic characteristics of precipitation at UG. From the non–standardized UG $\delta^{18}O$–stack a statistically significant positive trend of s = +0.058 ‰ a^{-1} (p–value < 0.0001) has been found, suggesting that the UG region might have experienced a slight warming at least since 1980. When using standardized data, the positive $\delta^{18}O$ trend is still preserved, however it is not statistically significant anymore (s = +0.003, p-value = 0.517). From this we infer that the regional increase in near–surface air temperature, if real, must have been small during the last 35 years. Apparently, the UG record is highly susceptible to minor changes in data processing and thus too short for drawing general conclusions on regional climate change. However, our finding based on standardized data is consistent with the absence of a clear regional warming on the AP since the late 1990s (Turner et al., 2016), although the tipping point from warming to cooling is not visible in the UG dataset. It is also in line with findings from ice cores retrieved from the Ronne–Filchner Ice Shelf and the Weddell Sea sector, respectively, that show no statistically significant trends in their stable water isotope time series (e.g. Foundation Ice Stream [Graf et al., 1999], Berkner Island [Mulvaney et al., 2002; Stenni et al., 2017]). A negative trend in air temperature has been observed in the instrumental record from Halley research station (1957-2000; Turner et al., 2005), whereas no trend has been found at Neumayer research station (1981-2010; Schlosser et al., 2014).

From time–series analysis of d excess annual means (S5) statistically significant positive trends have been found for SCH–2 (s = +0.085 ‰ a^{-1}, p–value < 0.0001) and PASO–1 (s = +0.016 ‰ a^{-1}, p–value = 0.002), whereas for DOTT–1 (s = –0.110 ‰

a^{-1}, p–value = 0.015) and SCH–1 (s = –0.052 ‰ a^{-1}, p–value < 0.0001) the d excess trend is negative. The BAL–1 d excess record exhibits no trend. In order to detect possible changes in the origin of precipitating air masses reaching the UG region a composite d excess record (UG d excess–stack) has been calculated (non–standardized and standardized) and analysed for the period 1980–2014 (Fig. 8). Neither the non–standardized nor the standardized record exhibits a statistically significant trend suggesting little change in the main moisture sources and the origin of air masses precipitating over the UG region since at least 1980.

4.1.2 Relation of stable water isotopes to meteorological data records

Linear regression between non–standardized seasonal means of UG near–surface air temperature and UG δ^{18}O for the period 2010–2015 (S6) revealed a statistically significant positive δ^{18}O–T relationship (δ^{18}O = 0.175*T–31.6, R^2 = 0.21, p–value = 0.03 [α = 0.05]). However, a proper inference of near–surface air temperatures from δ^{18}O values of precipitation in the UG region is not yet possible. This is due to (1) the shortness of the available near–surface air temperature record and (2) the arbitrary calculation of δ^{18}O seasonal means assuming that precipitation at the study site is evenly distributed throughout the year. Nevertheless, the presented δ^{18}O–T relationship confirms that δ^{18}O values and near–surface air temperatures in the UG region are positively interrelated, i.e. increasing air temperatures imply increasing δ^{18}O–values. Hence, they provide evidence that mean δ^{18}O values in the UG region can indeed be used as a proxy for near–surface air temperature at the site. In order to further test the robustness of this relationship, the UG δ^{18}O–stack (standardized) was spatially correlated with ERA–Interim near–surface air temperatures for the period 1980–2014 (Fig. 9a). Surprisingly, no correlation was found with near–surface air temperatures at the UG site, but with near–surface air temperatures further to the east (Coats Land). This might be due to the ERA–Interim model not capturing the local orography of the Ellsworth Mountains well and hence, not truly reflecting the local climate at the UG site, but rather the regional climate along the Weddell Sea coast.

4.1.3 Relation of stable water isotopes to large–scale climate modes and sea ice variability

Standardized mean annual d excess values exhibit a weak positive correlation with the SAM Index (0.40, p–value = 0.026; Table 3). Stronger contraction of the polar vortex during positive SAM phases facilitates the advection of warm and moist air from mid– and lower latitudes, i.e. from regions with higher SST and lower relative humidity towards Antarctica (Thompson and Wallace, 2000; Thompson and Solomon, 2002; Gillett et al., 2006). Hence atmospheric water vapour with higher d excess values is expected to reach Antarctica (Uemura et al., 2008; Stenni et al., 2010). Spatial correlations with ERA–Interim geopotential heights (850 mbar) calculated for the period 1980–2014 (Fig. 9c) confirm that increased geopotential heights above the mid–latitudes as occurring during positive SAM phases (Thompson and Wallace, 2000; Thompson and Solomon, 2002) imply increased d excess values of precipitation in the UG region. However, standardized mean annual δ–values show no correlation with the SAM Index (Table 3). Furthermore, none of the standardized isotopic values exhibits a correlation with the MEI Index (Table 3). Hence, oceanic circulation changes associated with the alternation between El Niño and La Niña events seem to have no visible influence on the stable water isotope composition of precipitation in the UG region.

Kohyama and Hartmann (2016) showed that the SAM Index is statistically significantly positively correlated with sea ice extent (SIE) in the Indian Ocean sector of Antarctica. When comparing SIE in the different Antarctic sectors (Weddell Sea, Bellingshausen–Amundsen Sea, Ross Sea, West Pacific, Indian Ocean) with standardized UG stacks of δ–values and d excess, the only (weak) correlation is found between UG d excess and SIE in the Indian Ocean sector (0.315, p–value = 0.074; Table 3). However, this correlation might be an artefact and does not necessarily indicate moisture transport from the Indian Ocean sector towards UG. Backward trajectory analyses with the HYSPLIT model (Fig. 10) suggest that the Weddell Sea sector is the dominant source region for precipitating air masses reaching the UG site. Spatial correlations with SIC yield a more specific regional picture of the interplay between sea ice distribution and UG moisture sources. We found that only SIC in the northern Weddell Sea exhibits a strong negative correlation with standardized mean annual δ^{18}O and d excess values in the UG region (r < –0.6; Fig. 11a and b) corroborating the results of the backward trajectory analyses. Thus, higher (lower) δ^{18}O and d excess values at the UG site correspond to a reduction (increase) in SIC in the northern Weddell Sea. Consequently, reduced SIC in the northern Weddell Sea implies enhanced availability of proximal moisture which would support higher δ–values in the UG region during low SIC phases. For a detailed interpretation of the negative correlation with UG d excess further data on the moisture sources' relative humidity is needed.

4.2 Spatial and temporal variability of accumulation rates and relation to sea ice and climate modes

4.2.1 Spatial and temporal variability of accumulation rates

For the overlapping period (1998–2013; Table 1) highest accumulation rates are observed at the DOTT-1 site that is located at the lowest elevation and closest to the sea. However, accumulation rates are very similar at the sites of SCH-1, SCH-2, BAL-1 and PASO-1, despite the clear differences in altitude and distance from the sea (Fig. 1b and Table 1). Accumulation rates have decreased at all sites throughout the respective record period, except at the PASO-1 site (Fig. 6). At SCH–1, SCH-2 and BAL–1 accumulation decreased at a rate of –0.002 m w.eq.a^{-1} (p-value = 0.032), –0.004 m w.eq.a^{-1} (p-value < 0.0001) and –0.003 m w.eq.a^{-1} (p-value = 0.006), respectively. The decrease is highest at the DOTT–1 site, but not statistically significant (s = –0.005 m w.eq.a^{-1}; p–value = 0.458). In contrast, accumulation exhibits a slight, albeit statistically significant increase at the PASO-1 site (s = +0.001 m w.eq.a^{-1}; p–value = 0). It seems that snow accumulation in the UG region is not directly related to altitude and distance to the sea. Furthermore, spatially varying accumulation trends likely reflect the strong influence of site–specific characteristics on accumulation rates, in particular the different exposure to wind drift. DOTT–1 and PASO–1 – the former located on an ice rise and the latter located on a high-altitude plateau – might be more exposed to wind drift than the sites of SCH–1, SCH–2 and BAL–1. The latter three are all located within U–shaped glacial valleys stretching from northwest to southeast (Fig. 1b), and, thus, are potentially better protected from the predominant south–westerly winds. Hence, here accumulation trends might be better preserved in the record.

Analogously to the UG δ^{18}O–stack a composite accumulation time series (non-standardized and standardized) has been constructed and analysed for the period that comprises at least three core records (1980-2014; excluding GUPA-1; Fig. 8). From the non-standardized accumulation record an average accumulation rate in the UG region of 0.25 m w.eq.a^{-1} has been

calculated. This value is roughly consistent with accumulation rates determined from stake measurements on UG (between 0.12 and 0.2 m w.eq.a^{-1}; Rivera et al., 2014), regional atmospheric model outputs (0.09–0.33 m w.eq.a^{-1}; van de Broeke et al., 2006), or from the close–by location of Patriot Hills (0.1 m w.eq.a^{-1}; Casassa et al., 1998) and the closest ITASE (International Trans–Antarctic Scientific Expedition) ice core 01–5 (0.39 m w.eq.a^{-1}; Kaspari et al., 2004).

5   The UG composite accumulation record – derived from both non- standardized and standardized time series – shows a slightly negative trend (Fig. 8; non-standardized: s = –0.001 m w.eq.a^{-1}, p–value = 0.006; standardized: s = -0.020, p-value = 0.001). This finding is in contrast to the positive precipitation trend observed on the AP (Turner et al., 2005; Frieler et al., 2015; Thomas et al., 2008; Thomas et al., 2017) and in coastal Ellsworth Land (Thomas et al., 2015).

10   **4.2.2 Relation of accumulation rates to sea ice variability and large–scale climate modes**

Backward trajectory analysis revealed that the Weddell Sea sector is the most likely moisture source region for UG (Fig. 10 and see above). Surprisingly, there does not appear to be a relationship between SIC in the Weddell Sea sector and snow accumulation at UG. Instead, there is a very weak positive correlation with SIC in the Bellingshausen Sea sector (Fig. 11c). Reduced sea ice in the Bellingshausen Sea sector, and the increased availability of surface level moisture, has been used to

15   explain the increases in snow accumulation along the AP and in coastal Ellsworth Land during the 20th century (Thomas et al., 2015). However, the UG site is considerably distant from the sea-ice edge and, thus, changes in sea ice appear to be less important for snow accumulation in this region. There is no correlation between snow accumulation at UG with either SAM or ENSO (Table 3). This suggests that snow accumulation in the UG region is likely not driven by large-scale modes of climate variability and that UG seems to be located in a transition zone between West and East Antarctic climate. The UG composite

20   accumulation record is only weakly correlated with ERA-Interim precipitation-evaporation time series at the site (Fig. 9b). Similar has been found for other firn and ice cores in the region (Thomas et al., 2017). This may be because the models used for the reanalysis are unable to capture the small orography of the Ellsworth Mountains, or be evidence of post-depositional processes at the firn core sites (wind erosion, snow deposition and/or drift).

25   **5. Conclusions**

In this study, we examined six firn cores from the Union Glacier region in the Ellsworth Mountains (79º46' S, 83º24' W) situated at the northern edge of the West Antarctic Ice Sheet. Based on all analysed firn cores, composite time series of δ–values, d excess and accumulation rates (non-standardized and standardized) were established for the entire Union Glacier region covering the period 1980–2014. A Local Meteoric Water Line was derived (δD = 8.02*δ^{18}O + 6.57, R^2 = 0.99) from

30   the co-isotopic relationship of all firn cores confirming the meteoric origin of snow and firn at UG.

The standardized composite δ^{18}O record revealed no statistically significant trend suggesting that regional changes in near-surface air temperature have been small at least since 1980. The absence of an isotope-temperature trend in the UG region is consistent with findings in the AP region and other parts of Antarctica.

Furthermore, it seems that standardized mean annual δ–values in the UG region are related to sea ice conditions in the northern Weddell Sea, but no concurrent relation exists with SAM and ENSO. Backward trajectory analyses confirm that the Weddell Sea sector is the likely dominant source region for precipitating air masses reaching the UG site. Standardized mean annual d excess values exhibit a weak positive correlation with the SAM Index implying that a more positive SAM facilitates higher d

5   excess values of precipitation in the UG region. However, no statistically significant trend has been found for the UG composite d excess record (both non-standardized and standardized) suggesting overall little change in the main moisture sources and the origin of air masses precipitating over the UG region since 1980.

On average annual accumulation in the UG region amounts to 0.25 m w.eq. with respect to the period 1980-2014. In contrast to stable water isotopes, mean annual accumulation in the UG region has slightly decreased since 1980 (non-standardized: -

10 0.001 m w.eq. a^{-1}; standardized: -0.020). There is no correlation between snow accumulation and either sea ice concentration or large-scale modes of atmospheric variability (SAM or ENSO). This confirms that the large increases in snow accumulation observed on the AP and in other coastal regions of Antarctica have not extended inland to the Ellsworth Mountains and that the UG region exhibits rather East than West Antarctic climate characteristics.

As the UG firn core records demonstrated to be are highly susceptible to minor changes in data processing, longer records and

15 deeper ice cores are essential to draw general and statistically more significant conclusions on climate change in the UG region.

Competing Interests.

The authors declare that they have no conflict of interest.

20 *Acknowledgements.*

We thank Antarctic Logistics and Expeditions and in particular Marc de Keyser for providing us with meteorological data from their AWS (station: Wx7) on Union Glacier. We gratefully acknowledge the PhD fellowship awarded to K. Hoffmann by the Elsa–Neumann scholarship of the state of Berlin, Germany.
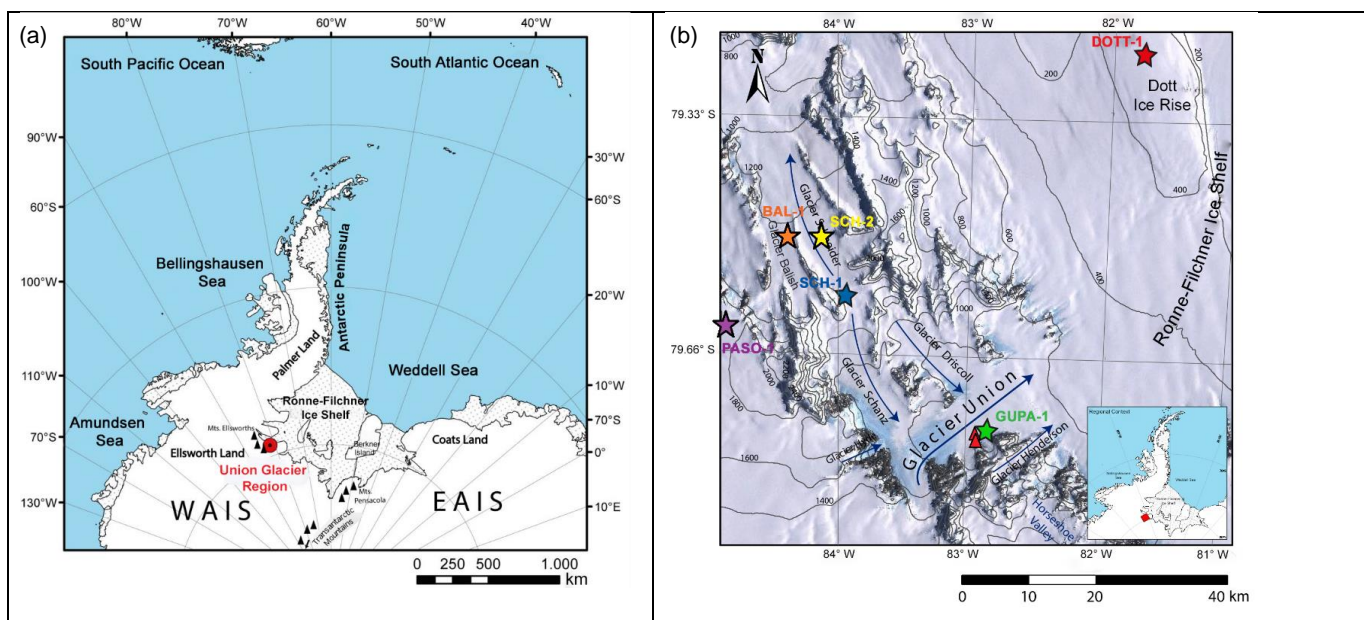
Figure 1a-b: Location of the UG region within Antarctica (a) and location of the drill sites of the six firn cores (GUPA–1, DOTT–1, SCH–1, SCH–2, BAL–1, PASO–1) within the UG region (b). The red triangles in (b) denote the location of two automatic weather stations on UG (stations: Wx7 and Arigony; further explanations in the text). The background image in (b) was extracted from the Landsat Image Mosaic of Antarctica (LIMA)
5   and the contour lines were obtained from the Radarsat Antarctic Mapping Project Digital Elevation Model, Version 2 (Liu et al., 2015).
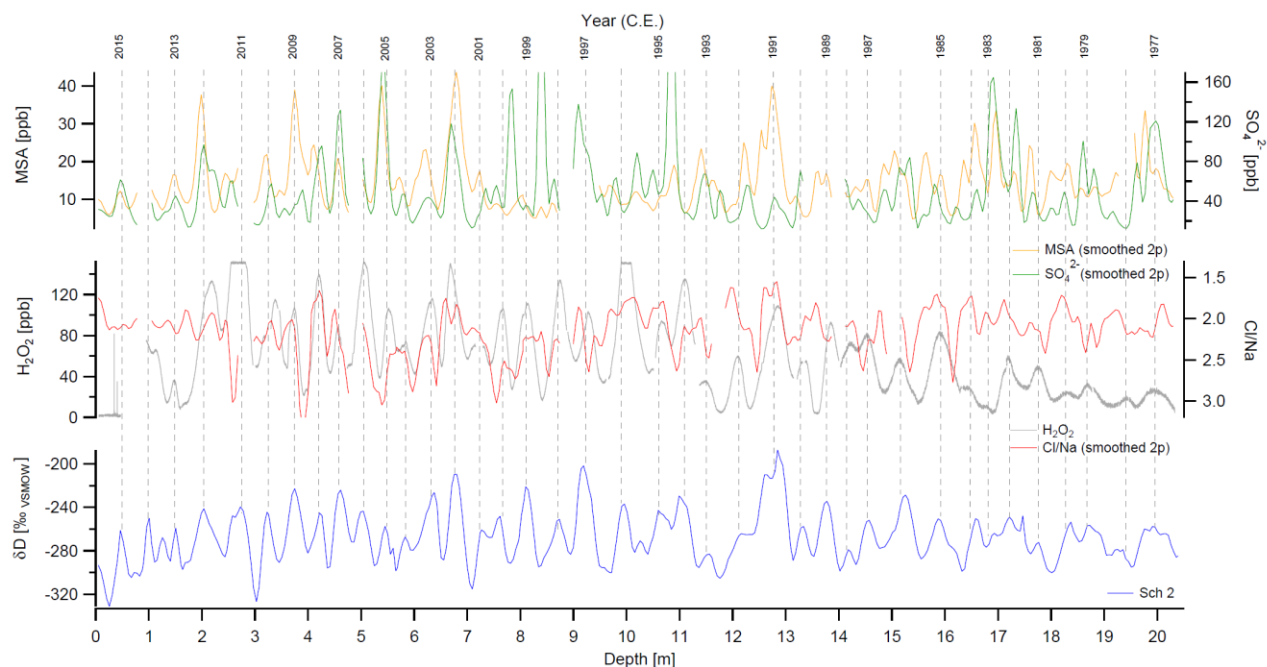
Figure 2: Age scale for firn core SCH–2 constructed by counting and inter–matching of maximum (minimum) peaks in CFA–derived profiles of stable water isotope composition (δD) and different chemical parameters (H_2O_2, Cl/Na, MSA and SO_4^{2-}).
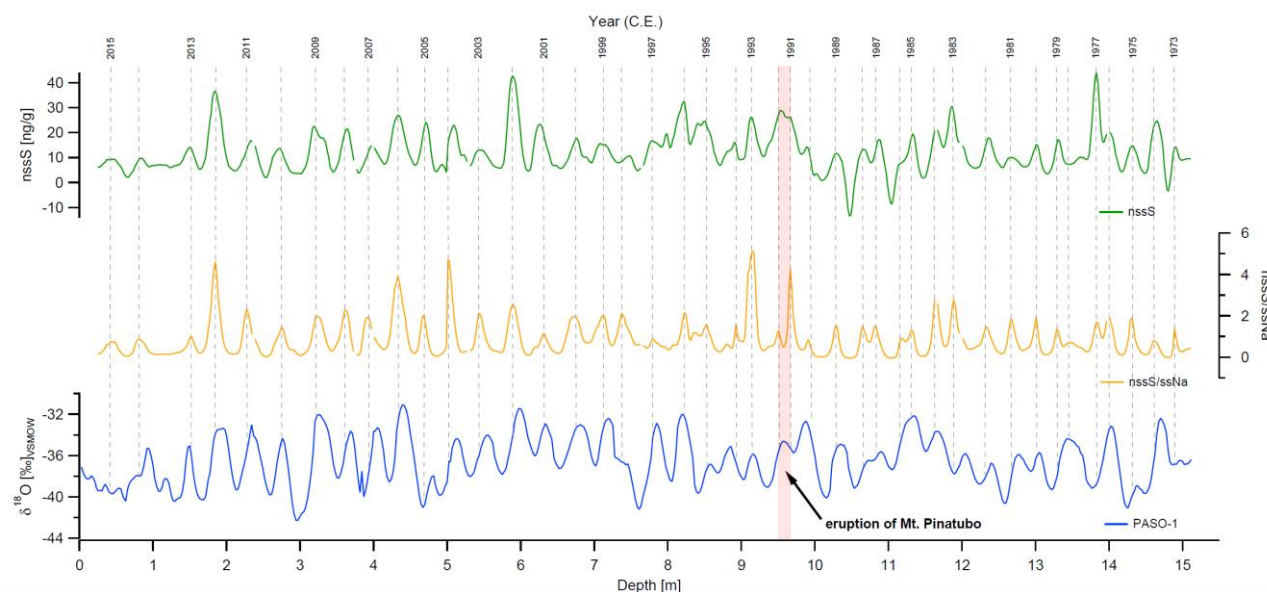
5   Figure 3: Age scale for firn core PASO–1 constructed by counting and inter–matching of maximum (minimum) peaks in profiles of stable water isotope composition ($δ^{18}O$) as obtained from discrete sample measurements and in CFA–derived profiles of nssS and nssS/ssNa, respectively. The year of the eruption of Mt. Pinatubo (1991) that is used as tie point for annual layer counting is highlighted.
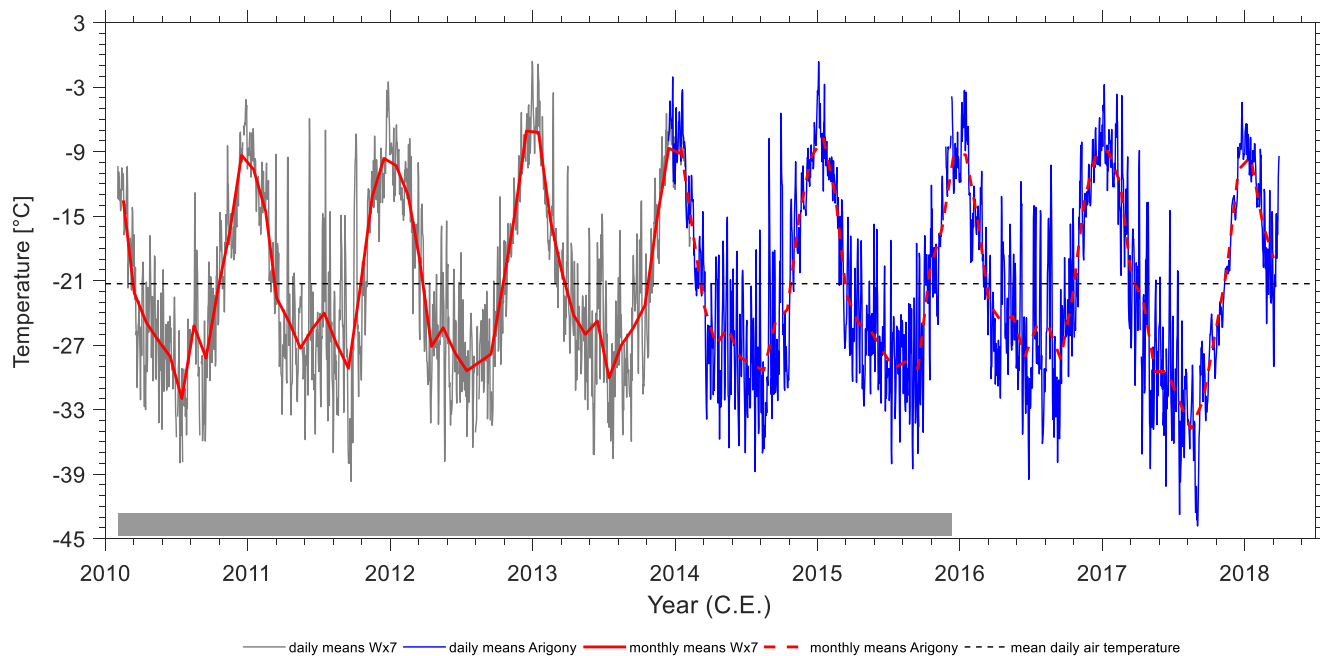
Figure 4: Composite record of mean daily and mean monthly air temperatures recorded at two nearby Union Glacier AWS sites (stations: Wx7, Arigony) from February 2010 to March 2018. The mean daily air temperature for the entire composite record period (–21.3°C; dashed black line) and the period overlapping with Union Glacier core records (February 2010 to November 2015; grey bar) are also indicated.
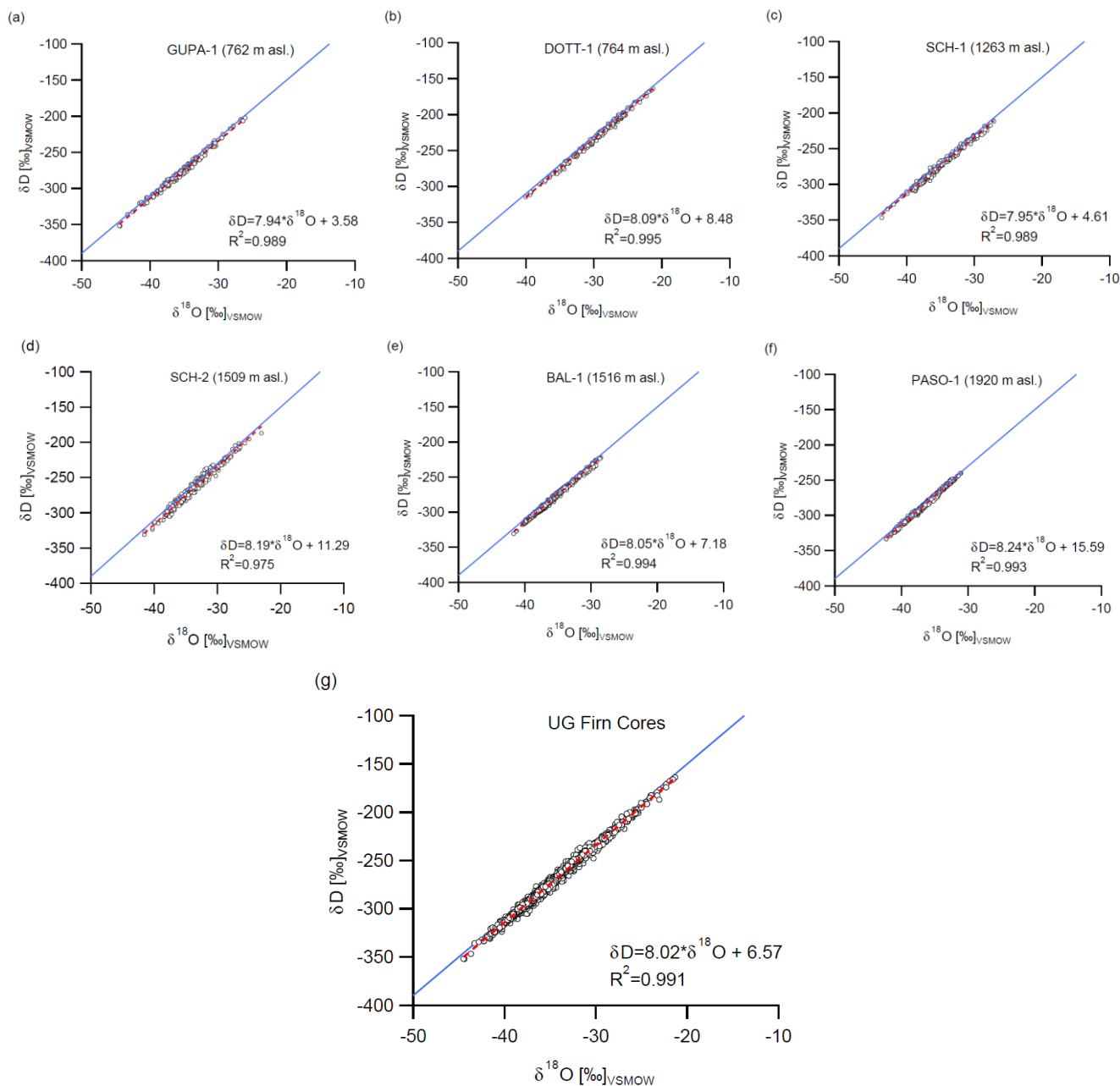
Figure 5a-g: Co–isotopic relationships for the six firn cores from Union Glacier (a-f). For each firn core the equation and the coefficient of determination (R^2) of the linear regression is shown. The Global Meteoric Water Line (GMWL) is indicated in blue. The composite co–isotopic relationship with its equation and R^2 that is referred to as the Local Meteoric Water Line (LMWL) of the Union Glacier region is also displayed (g).
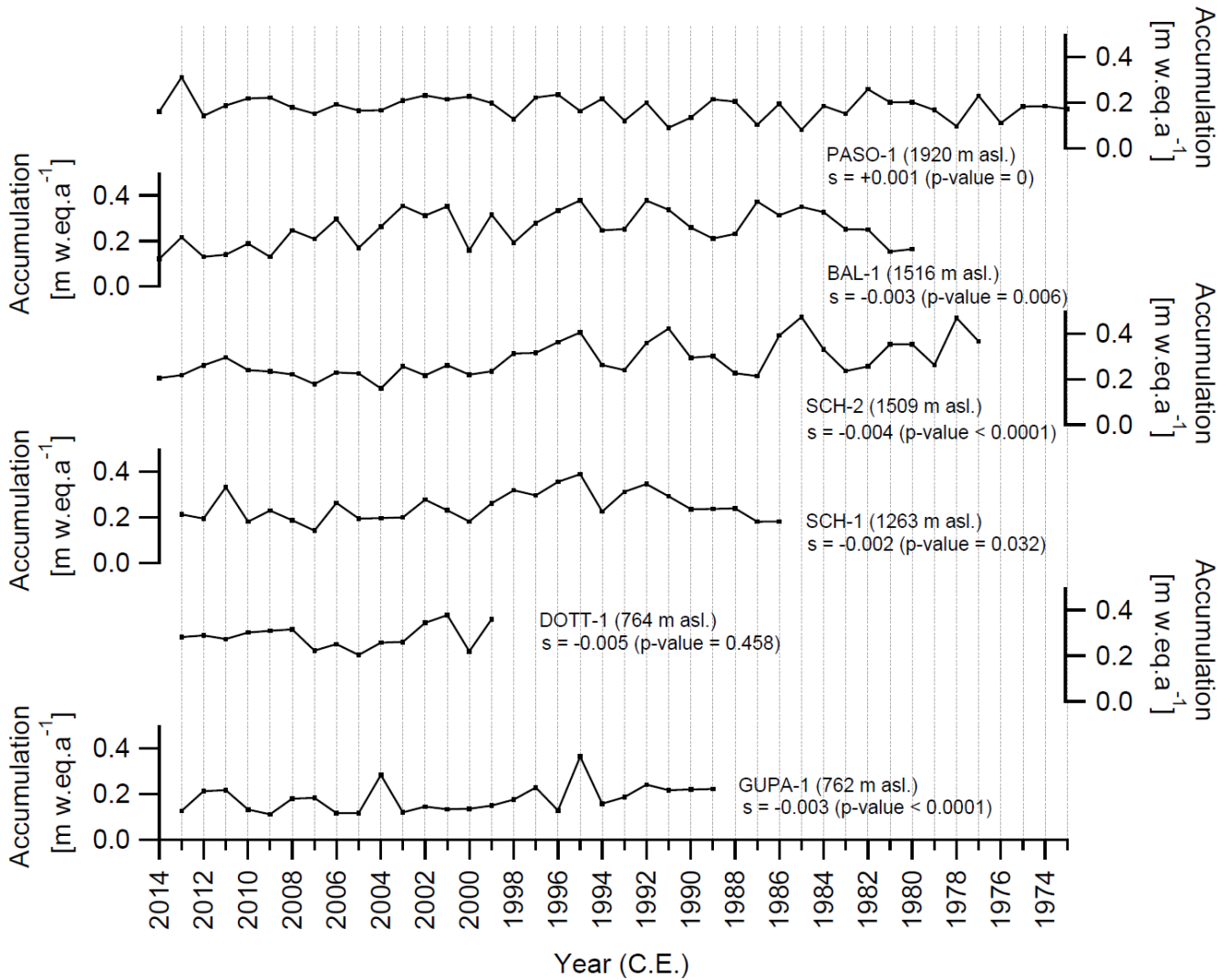
Figure 6: Accumulation rates at the sites of the six firn cores from Union Glacier for the period covered by the respective firn

core. Sen slopes (s) and p–values are given for all firn cores indicating that accumulation has decreased at most sites since the

5   beginning of the record period.
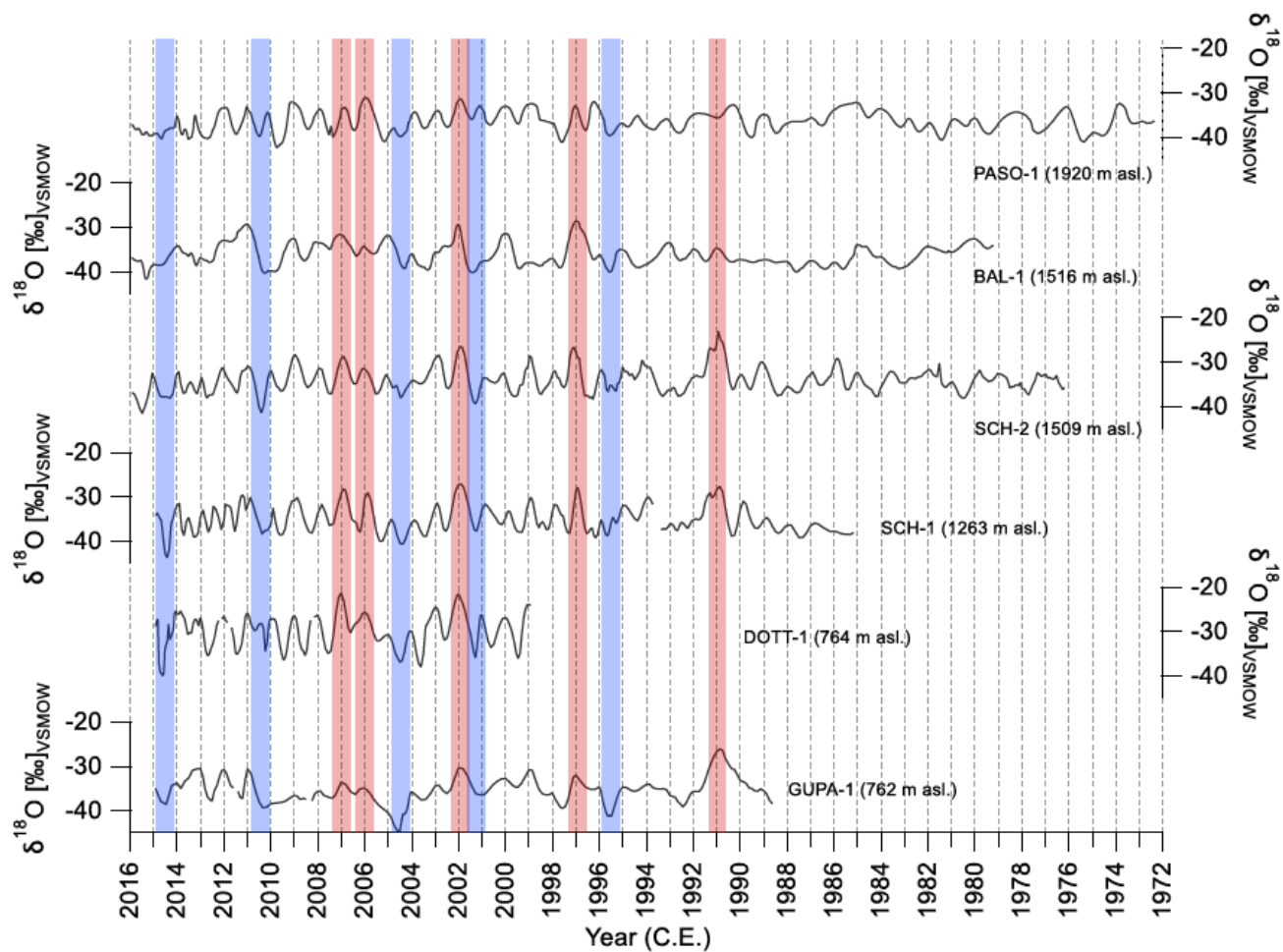
Figure 7: Profiles of the stable water isotope composition (δ^{18}O) of the six firn cores from Union Glacier with respect to time. Years with above–average maxima (warm summers) and minima (cold winters) – although not visible in all cores – are highlighted by red and blue shading, respectively.
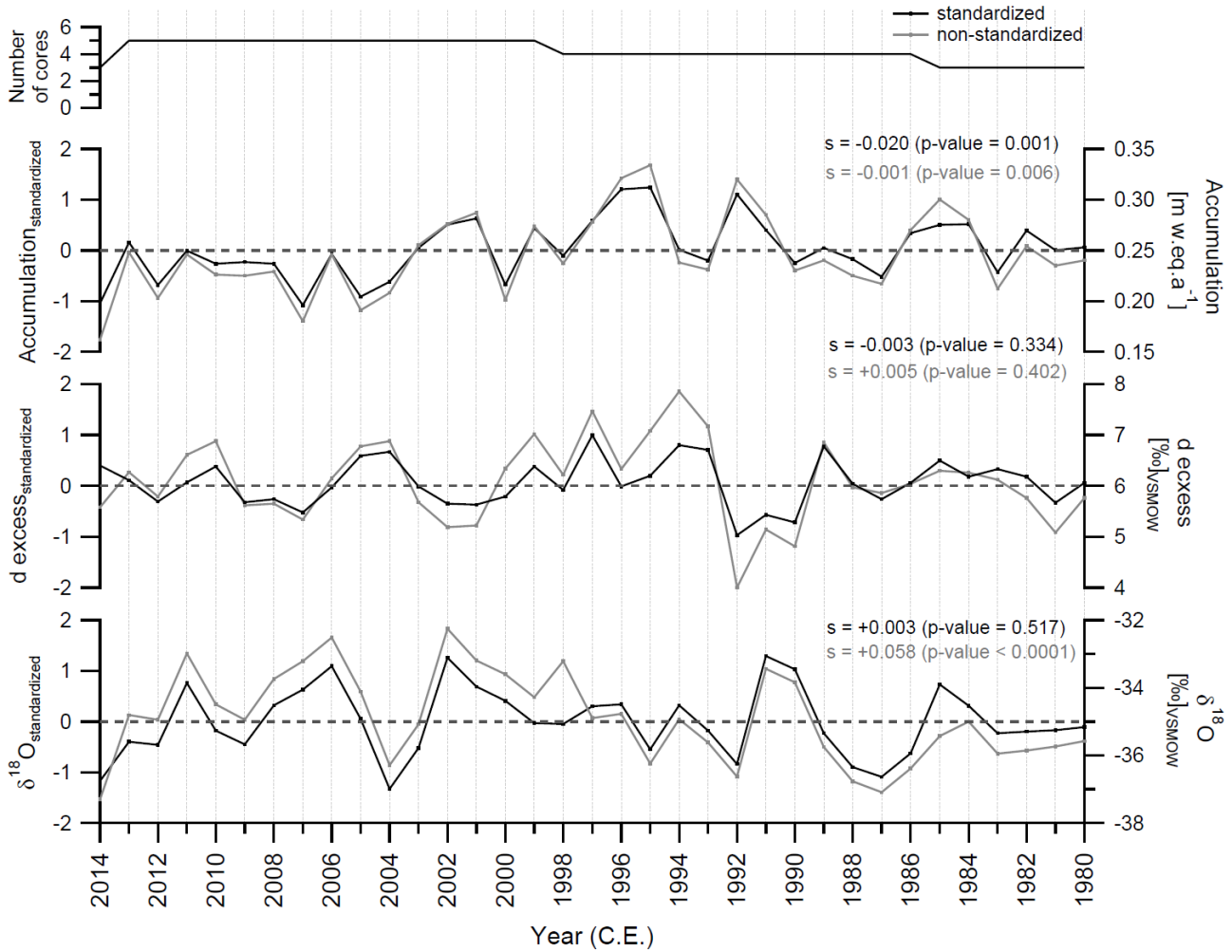
Figure 8: Composite records of mean annual $\delta^{18}O$, d excess and snow accumulation in the UG region for the period 1980-2014 derived from both non-standardized (grey) and standardized data (black). Sen slopes (s) and p–values are given for each record. Only mean annual snow accumulation exhibits a statistically significant negative trend for both non-standardized and standardized data.

(a)

(b)

(c)
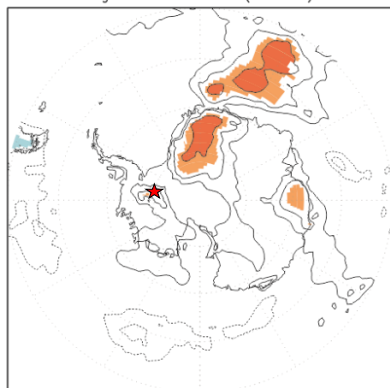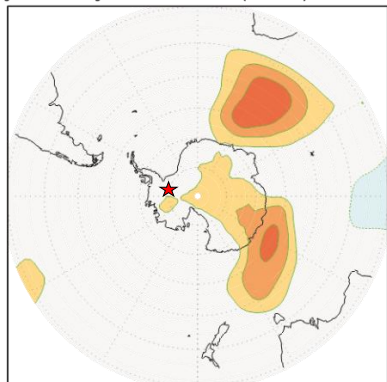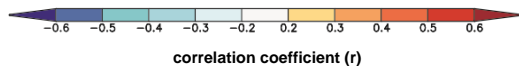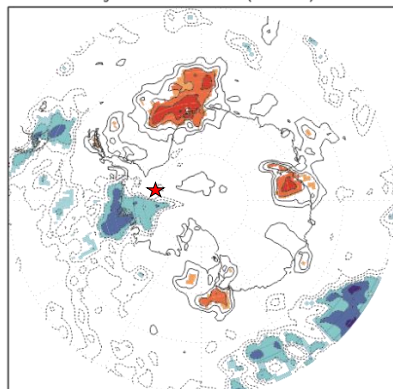
Figure 9a-c: Spatial correlation of annually averaged ERA-Interim (a) near-surface air temperatures (2 m), (b) geopotential heights (850 mbar) and (c) precipitation-evaporation with standardized mean annual (a) $\delta^{18}O$, (b) d excess and (c) snow accumulation in the UG region for the period 1980-2014. The red star denotes the location of the UG region. Only statistically significant correlations (p-value < 5%) are displayed. For (b) August -July annual averages (winter-winter) were considered as spatial correlations appear more significant than for December-November annual averages (calendar year).
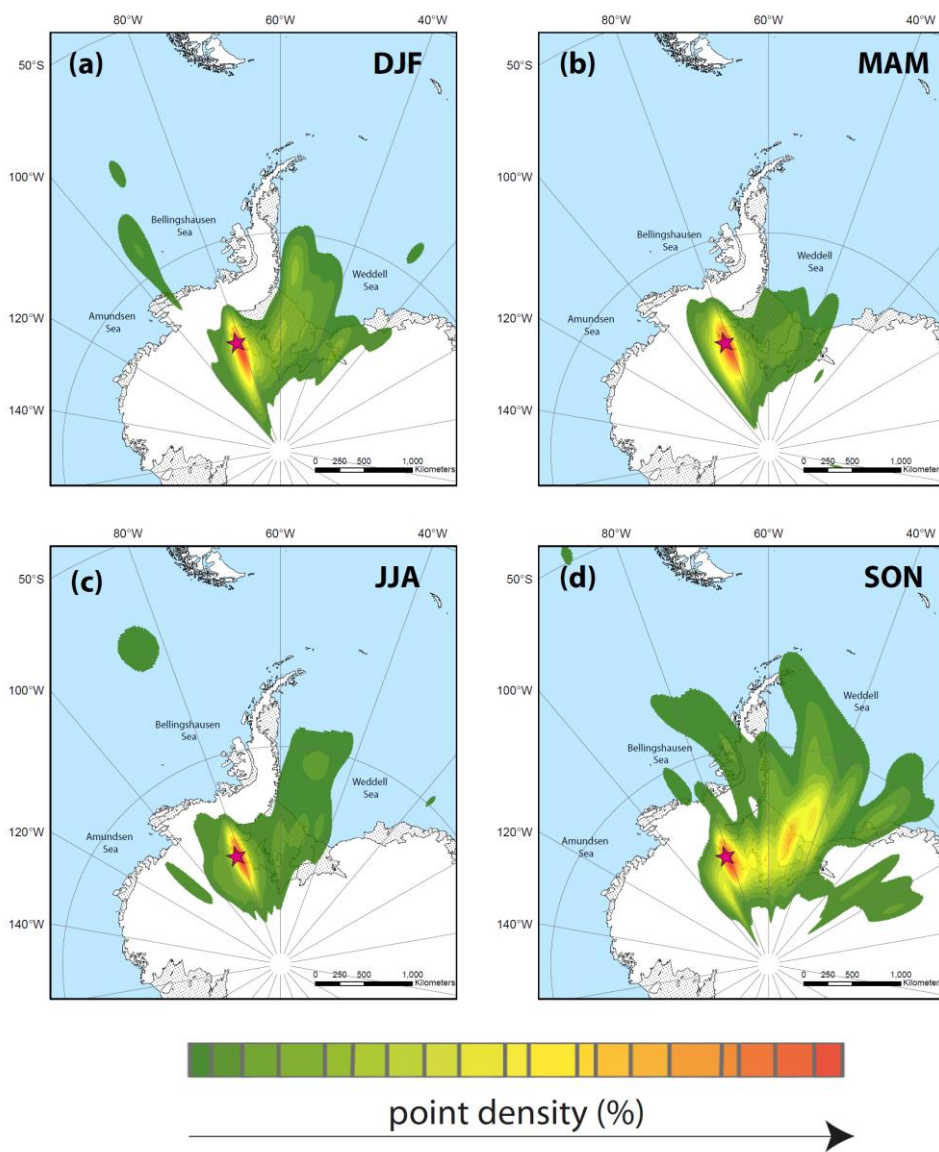
Figure 10a-d: Density distribution of 3–day backward trajectories transporting precipitating air masses towards the UG region (red star) as calculated for each season (DJF, MAM, JJA, SON) for the period 2010–2014 using the model HYSPLIT.
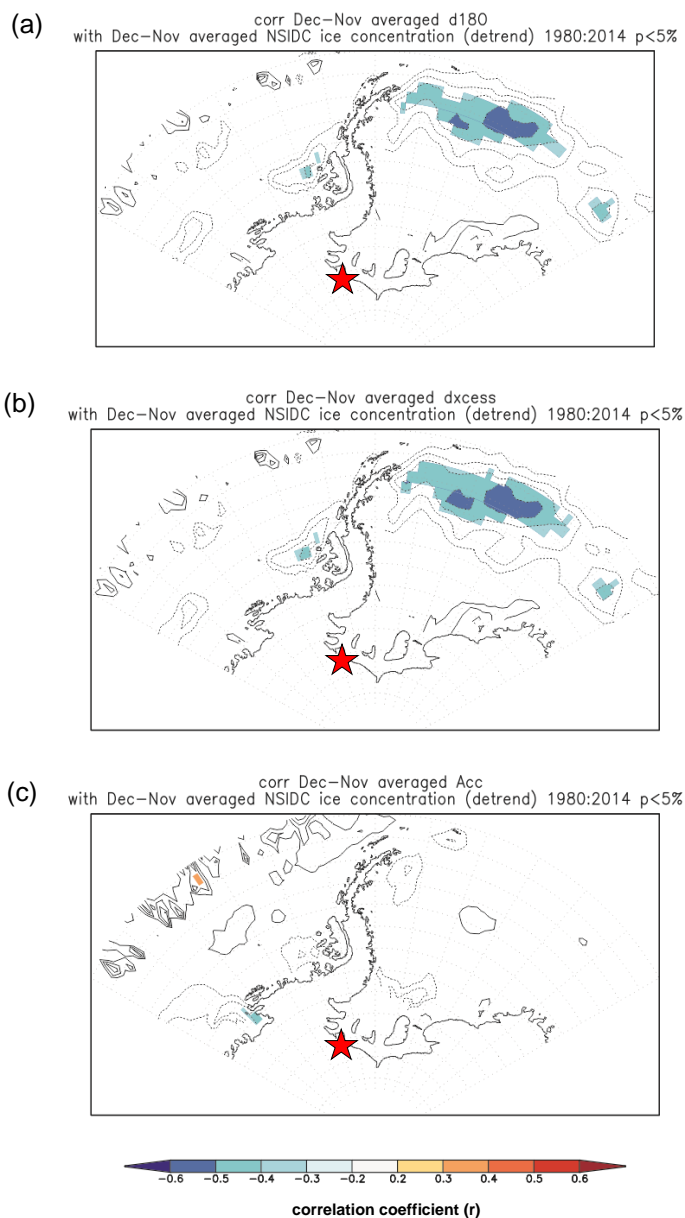
Figure 11a-c: Spatial correlations of standardized mean annual (a) δ^{18}O, (b) d excess and (c) snow accumulation in the UG region with mean annual sea ice concentrations in the Weddell and Bellingshausen Sea sectors for the period 1980-2014. The red star denotes the location of the UG region. Only statistically significant correlations (p-value < 5%) are shown.

Table 1: Details on drill locations and basic statistics of the stable water isotope composition and accumulation rates of the six firn cores retrieved from Union Glacier. Basic statistics are also given for the composite stable water isotope and accumulation records spanning the period 1980–2014. In addition, minimum, mean and maximum values of stable oxygen isotope annual means and accumulation rates are given for the period covered by all cores (1999–2013).

Firn Core	GUPA–1	DOTT–1	SCH–1	SCH–2	BAL–1	PASO–1
Coordinates	79°46'07.00''S 82°54'33.44''W	79°18'38.84''S 81°39'09.33''W	79°31'14.02''S 84°08'56.48''W	79°33'17.76''S 84°03'11.46''W	79°31'27.69''S 84°26'32.09''W	79°38'00.68''S 85°00'22.51''W
Altitude (m a.s.l.)	762	764	1263	1509	1516	1920
Depth (m)	9.58	9.57	14.13	20.25	17.28	15.04
Drilling date	Nov 2014	Nov 2014	Nov 2014	Nov 2015	Nov 2015	Nov 2015
$\delta^{18}O$ [‰]						
Min	–44.5	–40.0	–43.7	–41.6	–41.7	–42.3
Mean	**–35.6**	**–29.9**	**–35.0**	**–34.1**	**–36.2**	**–36.6**
Max	–26.1	–21.3	–27.1	–23.1	–28.5	–31.1
Sdev	3.1	3.9	3.1	2.8	2.5	2.3
δD [‰]						
Min	–352.1	–314.6	–346.6	–331.2	–330.7	–333.7
Mean	**–278.6**	**–233.1**	**–273.3**	**–268.0**	**–284.1**	**–285.9**
Max	–202.5	–163.9	–211.2	–187.1	–222.3	–240.2
Sdev	25.0	31.6	24.6	23.2	20.3	19.2
d excess [‰]						
Min	–0.2	–2.3	–2.3	–5.6	–0.4	0.3
Mean	**5.8**	**5.8**	**6.5**	**4.9**	**5.5**	**7.0**
Max	11.8	10.5	15.5	17.2	9.7	11.5
Sdev	2.6	2.2	2.6	3.7	1.6	1.7
slope of co–isotopic relationship	7.94	8.09	7.95	8.19	8.05	8.24
n (samples)	190	189	280	418	675	596
$\delta^{18}O$ [‰] of annual means for 1999–2013						
Min	–41.08	–33.45	–37.82	–36.58	–38.81	–38.69
Mean	**–35.38**	**–29.71**	**–34.91**	**–34.03**	**–36.11**	**–36.42**
Max	–29.25	–26.99	–32.09	–30.51	–31.49	–32.69
Accumulation [m w.eq.a^{-1}]	1989–2013	1999–2013	1986–2013	1977–2014	1980–2014	1973–2014
Min	0.111	0.203	0.142	0.159	0.121	0.080
Mean	**0.180**	**0.284**	**0.247**	**0.285**	**0.253**	**0.181**
Max	0.364	0.378	0.390	0.472	0.378	0.311

Sdev	0.061	0.052	0.064	0.078	0.079	0.048
Accumulation [m w.eq.a⁻¹] for 1999–2013					
Min	0.111	0.203	0.142	0.159	0.130	0.141
Mean	**0.158**	**0.284**	**0.219**	**0.229**	**0.231**	**0.200**
Max	0.284	0.378	0.333	0.295	0.353	0.311

Table 2: Dating results for the six firn cores from Union Glacier based on annual layer counting (stable water isotopes and glacio–chemistry) and core inter–matching taking SCH–2 as reference.

Firn Core	Period	Total number of years (δ^{18}O/δD summer maxima)
GUPA–1	1989–2014	26
DOTT–1	1999–2014	16
SCH–1	1986–2014	29
SCH–2	1977–2015	39
BAL–1	1980–2015	36
PASO–1	1973–2015	43

Table 3: Results of cross–correlation analysis for standardized stable water isotope and accumulation composite records from Union Glacier and time series of SAM Index, Multivariate ENSO Index (MEI) and sea ice extent (SIE) in five different Antarctic sectors. Cross–correlations were calculated considering the record period that is covered by a minimum of three firn cores (1980–2014). Prominent correlations are marked bold and if statistically significant (p–value < 0.01, α = 0.05) in red and bold.

1980–2014	δ¹⁸O	δD	d excess	Accumulation	SAM Index	MEI	SIE Weddell	SIE Bellingshausen-Amundsen	SIE Indian Ocean	SIE West Pacific	SIE Ross
δ¹⁸O	1	**0.995**	–0.214	0.194	–0.089	**–0.200**	-0.247	-0.116	-0.036	0.061	0.116
p–value	0	0	0.217	0.264	0.613	0.249	0.165	0.521	0.841	0.737	0.520
δD		1	–0.128	0.190	–0.054	**–0.214**	-0.264	-0.106	-0.003	0.085	0.119
p–value		0	0.464	0.275	0.758	0.218	0.138	0.559	0.985	0.639	0.511
d excess			1	–0.071	**0.376**	0.024	-0.205	0.103	**0.315**	0.169	-0.068
p–value			0	0.687	0.026	0.890	0.253	0.570	0.074	0.348	0.707
Accumulation				1	–0.139	0.039	-0.046	0.127	**-0.310**	-0.024	-0.143
p–value				0	0.427	0.826	0.799	0.483	0.080	0.896	0.429
SAM Index					1	–0.101	-0.223	-0.213	**0.629**	**0.403**	**0.390**
p–value					0	0.563	0.211	0.233	0	0.020	0.025
MEI						1	0.165	0.171	**-0.411**	0.025	**-0.512**
p–value						0	0.358	0.343	0.018	0.891	0.002

References

Abram, N.J., Mulvaney, R. and Arrowsmith, C.: Environmental signals in a highly resolved ice core from James Ross Island, Antarctica, J. Geophys. Res., 116, D20116, doi:10.1029/2011JD016147, 2011.

Bromwich, D.H., Nicolas, J.P., Monaghan, A.J., Lazzara, M.A., Keller, L.M., Weidner, G.A. and Wilson, A.B.: Central West Antarctica among the most rapidly warming regions on Earth, Nat. Geosci., 6, 139–145, doi:10.1038/NGEO1671, 2013.

Casassa, G., Brecher, H.H., Cárdenas, C. and Rivera, A.: Mass balance of the Antarctic ice sheet at Patriot Hills, Ann. Glaciol.,
10   27, 130–134, 1998.

Clark, I.D. and Fritz, P.: Environmental Isotopes in Hydrogeology, CRC Press LLC, Boca Raton, New York, USA, 1997.

Comiso, J.: Bootstrap Sea Ice Concentrations from Nimbus–7 SMMR and DMSP SSM/I–SSMIS, Version 3 [NSIDC–0079],
15   Boulder, Colorado, USA, NASA National Snow and Ice Data Center Distributed Active Archive Center, doi:10.5067/7Q8HCCWS4I0R [accessed 23rd July 2018], 2017.

Cook, A.J. and Vaughan, D.G.: Overview of areal changes of the ice shelves on the Antarctic Peninsula over the past 50 years, The Cryosphere, 4, 77–98, 2010.

Coplen, T. B. and Wassenaar, L.I.: LIMS for Lasers 2015 for achieving long–term accuracy and precision of δ^2H, $\delta^{17}O$, and $\delta^{18}O$ of waters using laser absorption spectrometry, Rapid. Commun. Mass. Sp., 29, 2122–2130, doi:10.1002/rcm.7372, 2015.

25   Craig, H.: Isotopic Variations in Meteoric Waters, Science, 133, 1702–1703, doi:10.1126/science.133.3465.1702, 1961.

Dansgaard, W.: Stable isotopes in precipitation, Tellus, 16, 436–468, doi:10.1111/j.2153–3490.1964.tb00181.x, 1964.

Dee, D.P., Uppala, S.M., Simmons, A.J., Berrisford, P., Poli, P., Kobayashi, S., Andrae, U., Balmaseda, M.A., Balsamo, G.,
30   Bauer, P., Bechtold, P., Beljaars, A.C.M., van de Berg, L., Bidlot, J., Bormann, N., Delsol, C., Dragani, R., Fuentes, M., Geer, A.J., Haimberger, L., Healy, S.B., Hersbach, H., Hólm, E.V., Isaksen, L., Kållberg, P., Köhler, M., Matricardi, M., McNally, A.P., Monge-Sanz, B.M., Morcrette, J.-J., Park, B.-K., Peubey, C., de Rosnay P., Tavolato, C., Thépaut, J.-N. and Vitart, F.: The ERA-Interim reanalysis: configuration and performance of the data assimilation system, Q. J. Roy. Meteor. Soc., 137, 553-597, doi:10.1002/qj.828, 2011.

Diaz, H.F. and Markgraf, V.: El Niño. Historical and Paleoclimatic Aspects of the Southern Oscillation, Cambridge University Press, Cambridge, UK, 1992.

5   Diaz, H.F. and Markgraf, V.: El Niño and the Southern Oscillation. Multiscale Variability and Global and Regional Impacts, Cambridge University Press, Cambridge, UK, 2000.

Ding, Q., Steig, E.J., Battisti, D.S. and Küttel, M.: Winter warming in West Antarctica caused by central tropical Pacific warming, Nat. Geosci., 4, 398–403, doi:10.1038/NGEO1129, 2011.

Draxler, R.R. and Hess, G.D.: An Overview of the HYSPLIT_4 Modelling System for Trajectories, Dispersion, and Deposition, Aust. Meteorol. Mag., 47, 295–308, 1998.

Fernandoy, F., Tetzner, D., Meyer, H., Gacitúa, G., Hoffmann, K., Falk, U., Lambert, F. and MacDonell, S.: New insights
15   into the use of stable water isotopes at the northern Antarctic Peninsula as a tool for regional climate studies, The Cryosphere, 12, 1069–1090, doi:10.5194/tc–12–1069–2018, 2018.

Freitag, J., Kipfstuhl, S. and Laepple, T.: Core–scale radioscopic imaging: a new method reveals density–calcium link in Antarctic firn, J. Glaciol., 59, 1009–1014, doi:10.3189/2013JoG13J028, 2013.

Frieler, K., Clark, P.U., He, F., Buizert, C., Reese, R., Ligtenberg, S.R.M., van den Broeke, M.R., Winkelmann, R. and Levermann, A.: Consistent evidence of increasing Antarctic accumulation with warming, Nat. Clim. Change, doi:10.1038/NCLIMATE2574, 2015.

25   Gillett, N.P., Kell, T.D. and Jones, P.D.: Regional climate impacts of the Southern Annular Mode, Geophys. Res. Lett., 33, L23704, doi:10.1029/2006GL027721, 2006.

Gillett, N.P., Stone, D.A., Stott, P.A., Nozawa, T., Karpechko, A.Y., Hegerl, G.C., Wehner, M.F. and Jones, P.D.: Attribution of polar warming to human influence, Nat. Geosci., 1, 750–754, doi:10.1038/ngeo338, 2008.

Graf, W., Reinwarth, O., Oerter, H., Mayer, C. and Lambrecht, A.: Surface accumulation on Foundation Ice Stream, Antarctica, Ann. Glaciol., 29, 23–28, 1999.

Hellmer, H.H., Kauker, F., Timmermann, R., Determann, J. and Rae, J.: Twenty–first–century warming of a large Antarctic ice–shelf cavity by a redirected coastal current, Nature, 485, 225–228, doi:10.1038/nature11064, 2012.

Hellmer, H.H., Kauker, F., Timmermann, R. and Hattermann, T.: The Fate of the Southern Weddell Sea Continental Shelf in a Warming Climate, J. Climate, 30, 4337–4350, doi:10.1175/JCLI–D–16–0420.1, 2017.

Hosking, J. S., Orr, A., Marshall, G.J., Turner, J. and Phillips, T.: The influence of the Amundsen–Bellingshausen Seas Low on the Climate of West Antarctica and Its Representation in Coupled Climate Model Simulations, J. Climate, 26, 6633–6648, doi:10.1175/JCLI–D–12–00813.1, 2013.

Joughin, I. and Alley, R.B.: Stability of the West Antarctic ice sheet in a warming world, Nat. Geosci., 4, 506–513, doi:10.1038/NGEO1194, 2011.

Karoly, D.J.: Southern Hemisphere Circulation Features Associated with El Niño–Southern Oscillation Events, J. Climate, 2, 1239–1252, doi: 10.1175/1520–0442(1989)002<1239:SHCFAW>2.0.CO;2, 1989.

Kaspari, S., Mayewski, P.A., Dixon, D.A., Spikes, V.B., Sneed, S.B., Handley, M.J. and Hamilton, G.S.: Climate Variability in West Antarctica derived from annual accumulation–rate records from ITASE firn/ice cores, Ann. Glaciol., 39, 585–594, 2004.

Kendall, M.G.: Rank correlation methods, Griffin, London, UK, 1975.

Kohyama, T. and Hartmann, D.L.: Antarctic Sea Ice Response to Weather and Climate Modes of Variability, J. Climate, 29, 721–741, doi:10.1175/JCLI–D–15–0301.1, 2016.

L'Heureux, M.L. and Thompson, D.W.J.: Observed Relationships between the El Niño–Southern Oscillation and the Extratropical Zonal–Mean Circulation, J. Climate, 19, 276–287, doi:10.1175/JCLI3617.1, 2006.

Limpasuvan, V. and Hartmann, D.L.: Eddies and the annular modes of climate variability, Geophys. Res. Lett., 26, 3133–3136, 1999.

Liu, H., Jezek, K.C., Li, B. and Zhao, Z.: Radarsat Antarctic Mapping Project Digital Elevation Model, Version 2 [NSIDC-0082], Boulder, Colorado, USA, NASA National Snow and Ice Data Center Distributed Active Archive Center, doi:10.5067/8JKNEW6BFRVD [accessed 3rd August 2018], 2015.

Mann, H.B.: Nonparametric tests against trend, Econometrica, 13, 245–259, 1945.

Marshall, G.J.: Trends in the Southern Annular Mode from Observations and Reanalyses, J. Climate, 16, 4134–4143, doi: 10.1175/1520-0442(2003)016<4134:TITSAM>2.0.CO;2, 2003.

Marshall, G.J., Orr, A., van Lipzig, N.P.M. and King, J.C.: The Impact of a Changing Southern Hemisphere Annular Mode on Antarctic Peninsula Summer Temperatures. J. Climate, 19, 5388-5404, doi: 10.1175/JCLI3844.1, 2006.

Marshall, G.J.: Half–century seasonal relationships between the Southern Annular Mode and Antarctic temperatures, Int. J.
10 Climatol., 27, 373–383, doi:10.1002/joc.1407, 2007.

McConnell, J.R., Lamorey, G.W., Lambert, S.W., Taylor, K.C.: Continuous Ice–Core Chemical Analyses Using Inductively Coupled Plasma Mass Spectrometry, Environ. Sci. Technol., 36, 7–11, doi:10.1021/es011088z, 2002.

15 McConnell, J.R., Edwards, R., Kok, G.L., Flanner, M.G., Zender, C.S., Saltzman, E.S., Banta, J.R., Pasteris, D.R., Carter, M.M., Kahl, J.D.W.: 20th–Century Industrial Black Carbon Emissions Altered Arctic Climate Forcing, Science, 317, 1381–1384, doi: 10.1126/science.1144856, 2007.

Merlivat, L. and Jouzel, J.: Global Climatic Interpretation of the Deuterium–Oxygen 18 Relationship for Precipitation, J.
20 Geophys. Res., 84, 5029–5033, 1979.

Mulvaney, R., Oerter, H., Peel, D.A., Graf, W., Arrowsmith, C., Pasteur, E.C., Knight, B., Littot, G.C. and Miners, W.D.: 1000 year ice–core records from Berkner Island, Antarctica, Ann. Glaciol., 35, 45–51, 2002.

25 Pritchard, H.D. and Vaughan, D.G.: Widespread acceleration of tidewater glaciers on the Antarctic Peninsula, J. Geophys. Res., 112, F03S29, doi:10.1029/2006JF000597, 2007.

Raphael, M.N., Marshall, G.J., Turner, J., Fogt, R.L., Schneider, D., Dixon, D.A., Hosking, J.S., Jones, J.M. and Hobbs, W.R.: The Amundsen Sea Low. Variability, Change, and Impact on Antarctic Climate, Bull. Amer. Meteor. Soc., 97, 111–121,
30 doi:10.1175/BAMS–D–14–00018.1, 2015.

Rignot, E., Mouginot, J., Morlighem, M., Seroussi, H. and Scheuchl, B.: Widespread, rapid grounding line retreat of Pine Island, Thwaites, Smith, and Kohler glaciers, West Antarctica, from 1992 to 2011, Geophys. Res. Lett., 41, 3502–3509, doi:10.1002/2014GL060140, 2014.

Rivera, A., Zamora, R., Uribe, J.A., Jaña, R. and Oberreuter, J.: Recent ice dynamic and surface mass balance of Union Glacier in the West Antarctic Ice Sheet, The Cryosphere, 8, 1445–1456, doi:10.5194/tc–8–1445–2014, 2014.

5 Röthlisberger, R., Bigler, M., Hutterli, M., Sommer, S., Stauffer, B., Junghans, H. G., and Wagenbach, D.: Technique for continuous high–resolution analysis of trace substances in firn and ice cores, Environ. Sci. Technol., 34, 338–342, 2000.

Scambos, T. A., Berthier, E., Haran, T., Shuman, C.A., Cook, A.J., Ligtenberg. S.R.M. and Bohlander, J.: Detailed ice loss pattern in the northern Antarctic Peninsula: widespread decline driven by ice front retreats, The Cryosphere, 8, 2135–2145,
10 doi:10.5194/tc–8–2135–2014, 2014.

Schlosser, E., Anschütz, H., Divine, D., Martma, T., Sinisalo, A., Altnau, S. and Isaksson, E.: Recent climate tendencies on an East Antarctic ice shelf inferred from a shallow firn core network, J. Geophys. Res. Atmos., 119, 6549–6562, doi:10.1002/2013JD020818, 2014.

Sen, P.K.: Estimates of the Regression Coefficient Based on Kendall's Tau, J. Am. Stat. Assoc., 63, 1379–1389, 1968.
Steig, E.J., Schneider, D.P., Rutherford, S.D., Mann, M.E., Comiso, J.C. and Shindell, D.T.: Warming of the Antarctic ice–sheet surface since the 1957 International Geophysical Year, Nature, 457, 459–462, doi:10.1038/nature07669, 2009.

20 Steig, E.J., Ding, Q., White, J.W.C., Küttel, M., Rupper, S.B., Neumann, T.A., Neff, P.D., Gallant, A.J.E., Mayewski, P.A., Taylor, K.C., Hoffmann, G., Dixon, D.A., Schoenemann, S.W., Markle, B.R., Fudge, T.J., Schneider, D.P., Schauer, A.J., Teel, R.P., Vaughn, B.H., Burgener, L., Williams, J. and Korotkikh, E.: Recent climate and ice sheet changes in West Antarctica compared with the past 2,000 years, Nat. Geosci., 6, 372–375, doi:10.1038/NGEO1778, 2013.

25 Stein, A.F., Draxler, R.R, Rolph, G.D., Stunder, B.J.B., Cohen, M.D. and Ngan, F.: NOAA's HYSPLIT Atmospheric Transport and Dispersion Modeling System, B. Am. Meteorol. Soc., 96, 2059–2077, doi:10.1175/BAMS–D–14–00110.1, 2015.

Stenni, B., Masson–Delmotte, V., Selmo, E., Oerter, H., Meyer, H., Röthlisberger, R., Jouzel, J., Cattani, O., Falourd, S., Fischer, H., Hoffmann, G., Iacumin, P., Johnsen, S.J., Minster, B. and Udisti, R.: The deuterium excess records of EPICA
30 Dome C and Dronning Maud Land ice cores (East Antarctica), Quaternary. Sci. Rev., 29, 146–159, doi:10.1016/j.quascirev.2009.10.009, 2010.

Stenni, B., Curran, M.A.J., Abram, N.J., Orsi, A., Goursaud, S., Masson–Delmotte, V., Neukom, R., Goosse, H., Divine, D., van Ommen, T., Steig, E.J., Dixon, D.A., Thomas, E.R., Bertler, N.A.N., Isaksson, E., Ekaykin, A., Werner, M. and Frezzotti,

M.: Antarctic climate variability on regional and continental scales over the last 2000 years, Clim. Past, 13, 1609–1634, doi:10.5194/cp–13–1609–2017, 2017.

Thomas, E.R., Marshall, G.J. and McConnell, J.R.: A doubling in snow accumulation in the western Antarctic Peninsula since 5 1850, Geophys. Res. Lett., 35, L01706, doi:10.1029/2007GL032529, 2008.

Thomas, E.R., Dennis, P.F., Bracegirdle, T.J. and Franzke, C.: Ice core evidence for significant 100–year regional warming on the Antarctic Peninsula, Geophys. Res. Lett., 36, L20704, doi:10.1029/2009GL040104, 2009.

10 Thomas, E.R., Bracegirdle, T.J., Turner, J. and Wolff, E.W.: A 308 year record of climate variability in West Antarctica, Geophys. Res. Lett., 40, 5492–5496, doi:10.1002/2013GL057782, 2013.

Thomas, E.R. and Bracegirdle, T.J.: Precipitation pathways for five new ice core sites in Ellsworth Land, West Antarctica, Clim. Dyn., 44, 2067–2078, doi:10.1007/s00382–014–2213–6, 2015.

Thomas, E.R., van Wessem, J.M., Roberts, J., Isaksson, E., Schlosser, E., Fudge, T.J., Vallelonga, P., Medley, B., Lenaerts, J., Bertler, N., van den Broeke, M., Dixon, D.A., Frezzotti, M., Stenni, B., Curran, M. and Ekaykin, A.A.: Regional Antarctic snow accumulation over the past 1000 years, Clim. Past, 13, 1491–1513, doi:10.5194/cp–13–1491–2017, 2017.

20 Thompson, D.W.J. and Wallace, J.M.: Annular Modes in the Extratropical Circulation. Part I: Month–to–Month Variability, J. Climate, 13, 1000–1016, doi:10.1175/1520–0442(2000)013<1000:AMITEC>2.0.CO;2, 2000.

Thompson, D.W.J. and Solomon, S.: Interpretation of Recent Southern Hemisphere Climate Change, Science, 296, 895–899, doi:10.1126/science.1069270, 2002.

Turner, J.: The El Niño–Southern Oscillation and Antarctica, Int. J. Climatol., 24, 1–31, doi:10.1002/joc.965, 2004.

Turner, J., Colwell, S.R., Marshall, G.J., Lachlan–Cope, T.A., Carleton, A.M., Jones, P.D., Lagun, V., Reid, P.A. and Iagovkina, S.: Antarctic climate change during the last 50 years, Int. J. Climatol., 25, 279–294, doi:10.1002/joc.1130, 2005.

Turner, J., Maksym, T., Phillips, T., Marshall, G.J. and Meredith, M.P.: The impact of changes in sea ice advance on the large winter warming on the western Antarctic Peninsula, Int. J. Climatol., 33, 852–861, doi:10.1002/joc.3474, 2013.

Turner, J., Lu, H., White, I., King, J.C., Phillips, T., Hosking, J.S., Bracegirdle, T.J., Marshall, G.J., Mulvaney, R. and Deb, P.: Absence of 21st century warming on Antarctic Peninsula consistent with natural variability, Nature, 535, 411–415, doi:10.1038/nature18645, 2016.

5 Uemura, R., Matsui, Y., Yoshimura, K., Motoyama, H. and Yoshida, N.: Evidence of deuterium excess in water vapor as an indicator of ocean surface conditions, J. Geophys. Res., 113, D19114, doi:10.1029/2008JD010209, 2008.

van Geldern, R. and Barth, J.A.C.: Optimization of instrument setup and post–run corrections for oxygen and hydrogen stable isotope measurements of water by isotope ratio infrared spectroscopy (IRIS), Limnol. Oceanogr. Meth., 10, 1024–1036, 10 doi:10.4319/lom.2012.10.1024, 2012.

Vaughan, D.G., Marshall, G.J., Connolley, W.M., Parkinson, C., Mulvaney, R., Hodgson, D.A., King, J.C., Pudsey, C.J. and Turner, J.: Recent rapid regional climate warming on the Antarctic Peninsula, Climate Change, 60, 243–274, 2003.

15 Wolter, K. and Timlin, M.S.: Monitoring ENSO in COADS with a Seasonally Adjusted Principal Component Index, in: Proceedings of the 17th Climate Diagnostics Workshop, Norman, Oklahoma, USA, 18–23 October 1992, 52–57, 1993.

Wolter, K. and Timlin, M.S.: Measuring the strength of ENSO events: How does 1997/98 rank?, Weather, 53, 315–324, 1998.

Yue, S. and Wang, C.Y.: The Mann–Kendall Test Modified by Effective Sample Size to Detect Trend in Serially Correlated Hydrological Series, Water. Resour. Manag., 18, 201–218, doi: 10.1023/B:WARM.0000043140.61082.60, 2004.